

Heavy-Metal Free Colloidal Quantum Dot Short-Wave Infrared Photodetectors and Image Sensors

Yongjie Wang¹, Lucheng Peng¹, Julien Schreier², Yu Bi², Andres Black², Stijn Goosens², Gerasimos Konstantatos^{1,3*}

¹ICFO-Institut de Ciències Fòniques, The Barcelona Institute of Science and Technology, Castelldefels, 08860 Barcelona, Spain.

²Qurv Technologies S.L., Castelldefels, 08860, Spain

³ICREA-Institució Catalana de Recerca i Estudis Avançats, Lluís Companys 23, 08010 Barcelona, Spain.

*e-mail: Gerasimos.Konstantatos@icfo.eu

Photodetectors that are sensitive in shortwave infrared (SWIR) range (1 μm - 2 μm) are of significant interest for applications in 3D, night and adverse weather imaging, machine vision, autonomous driving, among others. Currently available technologies in the SWIR rely on costly epitaxial semiconductors that are not monolithically integrated with CMOS electronics. Solution-processed quantum dots have been developed to address this challenge enabling low-cost manufacturing and facile monolithic integration on silicon in a back-end-of-line (BEOL) process. To date, colloidal quantum dot (CQD) materials to access the SWIR have been based on lead sulfide (PbS) and mercury telluride (HgTe) compounds imposing major regulatory concerns and impeding their deployment in consumer electronics. Here we report a novel synthetic method of environmentally friendly silver telluride quantum dots and their application in high-performance SWIR photodetectors. The CQD photodetector stack is entirely based on *Restriction of Hazardous Substance* (RoHS) compliant materials and exhibits a spectral range from 350 nm - 1600 nm, with room-temperature detectivity of the order 10^{12} Jones, 3dB bandwidth in excess of 0.1 MHz and linear dynamic range of over 118 dB. We further demonstrate,

for the first time, a monolithically integrated SWIR imager that is based on solution-processed, heavy-metal-free materials, paving the way of this technology to consumer electronics market.

Shortwave infrared (SWIR) light for sensing and imaging is of paramount importance owing to its unique characteristics: It is eye-safe; It can penetrate through fog, haze, and other atmospheric conditions, enabling imaging under adverse weather for automotive applications, environmental and remote sensing;¹⁻³ the presence of night glow under night in the SWIR enables passive night vision;⁴ visual imaging combined with infrared spectroscopy enables machine vision,³ bio-imaging,⁵⁻⁸ food and process quality inspection etc.^{9,10} Of particular relevance in the SWIR is the band around 1.35-1.4 μm that provides an eye-safe window, free of background light under day/night conditions enabling long-range LIDAR and 3D imaging for automotive and Augmented/Virtual Reality (AR/VR) applications.¹¹

In view of the huge market potential and the fact that established technologies to address the SWIR are based on highly costly and non-monolithic to silicon III-V technologies, significant efforts over the last 15 years have led to the demonstration of highly performing colloidal quantum dot photodetectors and image sensors.^{2,9,12-19} However, to date, the available CQD materials to access the SWIR are based on heavy metals of Pb and Hg that are ROHS regulated elements and currently prohibited for use in consumer electronics.

In this work we sought for a new heavy-metal free colloidal quantum dot semiconductor that would preserve the favorable properties of its heavy-metal counterparts in terms of broad bandgap tuneability and facile solution processing. We identified silver telluride quantum dots (Ag_2Te CQDs), as promising contender and after a thorough literature review we realized that while Ag_2Te CQDs have been synthesized and applied in bio-imaging applications as fluorophores in the near infrared²⁰⁻²³, its demonstration as an optoelectronic material with

tuneable and strong optical absorption akin to colloidal quantum dot materials has remained elusive. We posited that the origin of the challenge to achieve wide size tunability and thus broadband tunable optical properties, lies in the limited choice of tellurium precursors.^{23,24} Up to now, the most widely used tellurium precursor has been tri-alkyl-phosphine-tellurium ($R_3P = Te$), while phosphine has been suspected to adversely affect surface passivation, thereby the photoluminescence quantum yield.²³ At the same time phosphine-based ligands are known to bind strongly to Ag on the surface of QDs, and are therefore a not optimal ligand choice for CQDs that would need to undergo a ligand exchange process to render the films electrically conductive.^{23,25}

Phosphine-free Ag_2Te CQDs.

Various methods and precursors have been used to synthesize Ag_2Te QDs under different reaction conditions.^{20,22,26,27} However, achieving size tunability in these QDs has been challenging. Recently, large-sized Ag_2Te QDs with a photoluminescence peak exceeding 2000 nm were obtained using phosphine-induced ripening.²³ Nevertheless, obtaining a decent excitonic absorption peak above 1500 nm remains elusive, indicating insufficient control over size uniformity.²⁸ This limitation leads to energetic disorder and hinders charge transport, thereby compromising the performance of optoelectronic devices.²⁹⁻³¹ Therefore, there is an urgent need to develop a synthetic method capable of producing monodisperse Ag_2Te QDs with distinct excitonic peaks, which can be exploited in promising optoelectronic applications. Herein, we introduced a phosphine-free tellurium precursor that led us obtain Ag_2Te QDs with well-controlled size distribution and distinct excitonic peaks over a very broad range (800 nm to 2000 nm). Silver-oleylamine and tellurium-thiol complexes were used as precursors for hot injection. Thanks to the absence of phosphine, Ag_2Te QDs are stable in crude solution for hours under heating without showing Ostwald ripening, enabling us to easily tune sizes with

controlled precursor supply. As shown in Fig. 1a, the absorption spectrum of Ag₂Te QDs showed clear excitonic peaks, whose positions were controlled by reaction temperatures or continuous injection method (See Experimental Methods). The Ag₂Te QDs showed excellent air stability. With storing in air for two weeks, the absorption remained unaltered (Fig. S1). Intense photoluminescence was also observed under near infrared light excitation (Fig. S2). More importantly, we report here for the first time, Ag₂Te QDs with distinct excitonic peaks (peak-valley ratio > 1.2) over 1500 nm, which has been a formidable obstacle for phosphine-based methods.^{23,24}

X-ray photoelectron spectroscopy was first employed to examine the material composition and stoichiometry as function of QD size (Fig. S3). The Te to Ag ratio increases with the bandgap decreasing (size increasing), indicating a cation rich surface. Transmission electron microscopy (TEM) images (Fig. 1b-k) confirmed the controllable and tunable QD sizing from less than 2.9 nm to over 6.6 nm, with regular spherical shapes. High resolution TEM (Fig. 1l) showed high quality single-crystal characteristics with an evident lattice spacing of 0.23 nm, matching well with the XRD peak located at ~ 40° (Fig. S4). Thanks to the wide size and consequent bandgap tunability, we were able to extract the sizing curve from TEM size distribution and absorption spectra. The second derivatives of absorption spectrums were used to extract the multiple excitonic peaks (Fig. S5). The sizing curve was further fitted into equation:³²

$$E_g = \frac{1}{2} \left[E_0 + \sqrt{E_0^2 + 8E_0\alpha\pi^2 \frac{R_y a_0}{\epsilon_\infty d_0} \frac{e^{-\frac{d}{d_0}}}{(1 + e^{-\frac{d}{d_0}})^2}} \right]$$

where E_g is the size dependent bandgap, E_0 is the bulk bandgap, R_y is the Rydberg energy (13.606 eV), a_0 is the Bohr radius of hydrogen (0.053 nm), α is a prefactor accounting the size dispersion (~0.7), ϵ_∞ is the dielectric constant (here, ~16),³³ d_0 is the exciton Bohr diameter, d is the QD diameter. By fitting the first excitonic peak with QD sizes (Fig. 1m), the exciton

Bohr diameter was estimated to be ~10 nm, and the bulk bandgap E_0 was ~0.53 eV. We note that there exist various reports of the bulk bandgap of Ag₂Te with different values, which may stem from the various crystal phases and non-stoichiometry effects of this semiconductor compound.^{34–36} We believe further investigations, including theoretical calculations, would provide more insights.

Ag₂Te QDs SWIR photodiode.

Having obtained Ag₂Te QDs with good monodispersity, we aimed to implement them into a low-temperature, solution-processed, non-toxic SWIR photodiode device that is compatible with complementary metal–oxide–semiconductor (CMOS) readout integrated circuits (ROICs). Ag₂Te QDs photodiodes were initially fabricated with a configuration of ITO/SnO₂/Ag₂Te QDs/Au (Fig. 2a). However, devices showed poor rectification with high reverse bias dark current (Fig. 2c). Based on band positions from ultraviolet photoelectron spectroscopy (UPS, Fig. S6), we suspected that the poor device performance originates from severe interface recombination between SnO₂ and Ag₂Te QDs (Fig. 2b) and therefore sought to introduce a buffer layer that would act as an intermediate electron acceptor with lower carrier density than SnO₂. We found that inserting a buffer layer of AgBiS₂ nanocrystals between SnO₂ and Ag₂Te QDs improves drastically the device diode quality, leading to a reduced reverse bias dark current density down to ~ 2 $\mu\text{A}/\text{cm}^2$ @ -0.1V and ~6 $\mu\text{A}/\text{cm}^2$ @ -0.5 V (Fig. 2c and Fig. S7). In addition, the external quantum efficiency (EQE) showed substantial improvement with AgBiS₂ NCs buffer layer, together with a red-shift of EQE peak position, primarily due to optical effects (Fig. S8). The optimal photodiodes reached an EQE up to ~20% @1400 nm under 0 V bias (Fig. 2d) and 30% @-0.1 V (Fig. S9), while the devices without AgBiS₂ NCs showed peak EQE of only ~5%.

The linear dynamic range (LDR) of optimal Ag₂Te QD photodiode is further evaluated by varying the incident light intensity. As shown in Fig. 3a, the photocurrent maintained linearity with incident light power over a broad range and LDR is estimated to be over 118 dB, which compares favorably over PbS or HgTe QDs based photodiodes.^{17,37} Frequency dependent response was measured under zero bias, showing a -3dB bandwidth up to 110 kHz (Fig. 3b), which is in accordance with the fast rise and decay times of 1.3 μs and 3.3 μs under modulated light excitation (Fig. 3b inset). Frequency dependent noise spectral density was further measured with fast Fourier Transform (FFT) current transients for low frequency and a lock-in amplifier for high frequency range (Fig. S10). The obtained noise spectrum showed a 1/f noise dominating at low frequency and a generation-recombination noise at high frequency. The device reaches a noise floor of ~10⁻¹⁴ A Hz^{-0.5} at frequencies over 20 kHz. The measured room-temperature specific detectivity (D^*) was thus calculated according to:

$$D^* = \frac{R\sqrt{A\Delta f}}{i_n}$$

where A is the device area, Δf is the noise bandwidth (1 Hz), i_n being the noise spectral density. The frequency dependent D^* reached a maximum of ~ 3×10^{12} Jones at 20 kHz (Fig. S11). Moreover, the photodiode showed a D^* over 10^{12} Jones across a very broad spectral range covering from 350 nm to 1500 nm (Fig. 3c).

Furthermore, with the size tunability of Ag₂Te QDs developed here, we further extended the spectral peak to 1500 nm by employing larger QDs. The devices with 1520 nm absorption peak QDs showed responsivity of over 0.1 A/W at 1500 nm, -3 dB bandwidth of 220 kHz, D^* reaching 8.8×10^{11} Jones at 1500 nm (Fig. S12).

To the best of our knowledge, the photodiode devices reported here realized, for the first time, solution-processed, non-toxic shortwave infrared photodiodes with figures of merit on par with

other heavy-metal containing counterparts (Fig. 3d). These results further support the fact that Ag₂Te QDs emerges as a promising RoHS-compliant material for low-cost, high performance SWIR photodetector applications.

Ag₂Te CQDs SWIR imager.

Having developed a heavy-metal-free CQD photodetector, we were then motivated to demonstrate its potential in a SWIR image sensor use case. Prior to direct integration onto a read-out-integrated circuit (ROIC) we sought to optimize and evaluate its performance in a top-illuminated configuration on a mimic ITO-coated glass substrate (Fig. 4a) using patterned gold as bottom electrodes and 10 nm thin Au as a top semi-transparent electrode. The top-illuminated photodiode exhibited rectification characteristics under dark, albeit inferior to that of the bottom-illuminated devices. Due to the use of ultra-thin Au as a top electrode, forward bias larger than 0.1V led to device damage, preventing us to apply larger forward bias. The detector reaches an EQE ~9% at 1200 nm in short-circuit conditions, further increasing with reverse bias (Fig. 4b).

We then employed this stack for an image sensor by integrating it on a commercially available ROIC (see methods for details). Fig. 4d illustrates a schematic of the Ag₂Te CQD image sensor. Fig 4e illustrates the fabricated die in the electronic printed circuit board enclosure and Fig. 4f shows a zoomed-in photo of the die comprising the QD stack atop the ROIC. Fig. 4g-i illustrate a few examples of images taken using this imager under SWIR light exposure (900 nm – 2000 nm) along with photos taken with a standard mobile phone silicon-based camera. The figures show the transmission of silicon wafers under SWIR light as well as the possibility to visualize the content of plastic bottles that are opaque in the visible.

Conclusion.

In conclusion, we have first developed a novel synthetic method for size-tunable, phosphine-free Ag₂Te quantum dots. Photodiodes based on these Ag₂Te QDs further demonstrate compelling performance in shortwave infrared region with wide linear dynamic range over 118 dB, -3 dB bandwidth over 110 kHz, and a high room-temperature specific detectivity over 3×10^{12} Jones. We further employed heterogeneous monolithic integration of Ag₂Te CQD photodiodes onto Silicon ROICs to demonstrate for the first time a non-toxic, solution-processed SWIR imager operating at room temperature. The results reported here not only circumvent prior challenges in the synthesis of size-tunable, phosphine-free Ag₂Te QDs, but also unleash their potential as a novel ROHS-compliant infrared size-tuneable optoelectronic material. Finally, our work paves the way for the introduction of SWIR colloidal quantum dot technology in consumer electronics markets.

References

1. Guan, X. *et al.* Recent Progress in Short- to Long-Wave Infrared Photodetection Using 2D Materials and Heterostructures. *Adv. Opt. Mater.* **9**, 2001708 (2021).
2. Tang, X., Ackerman, M. M., Chen, M. & Guyot-Sionnest, P. Dual-band infrared imaging using stacked colloidal quantum dot photodiodes. *Nat. Photonics* **13**, 277–282 (2019).
3. Saran, R. & Curry, R. J. Lead sulphide nanocrystal photodetector technologies. *Nat. Photonics* **10**, 81–92 (2016).
4. Uwe Adomeit & Jürgen Krieg. Shortwave infrared for night vision applications: illumination levels and sensor performance. in vol. 9641 964104 (2015).
5. Wu, Z., Zhai, Y., Kim, H., Azoulay, J. D. & Ng, T. N. Emerging Design and Characterization Guidelines for Polymer-Based Infrared Photodetectors. *Acc. Chem. Res.* **51**, 3144–3153 (2018).
6. Naczynski, D. J. *et al.* Rare-earth-doped biological composites as in vivo shortwave infrared reporters. *Nat. Commun.* **4**, 2199 (2013).

7. Cosco, E. D. *et al.* Shortwave infrared polymethine fluorophores matched to excitation lasers enable non-invasive, multicolour in vivo imaging in real time. *Nat. Chem.* **12**, 1123–1130 (2020).
8. Bruns, O. T. *et al.* Next-generation in vivo optical imaging with short-wave infrared quantum dots. *Nat. Biomed. Eng.* **1**, 0056 (2017).
9. Konstantatos, G. & Sargent, E. H. Nanostructured materials for photon detection. *Nat. Nanotechnol.* **5**, 391–400 (2010).
10. García de Arquer, F. P., Armin, A., Meredith, P. & Sargent, E. H. Solution-processed semiconductors for next-generation photodetectors. *Nat. Rev. Mater.* **2**, 16100 (2017).
11. Goossens, S., Konstantatos, G. & Oikonomou, A. Colloidal Quantum Dot Image Sensors: Technology and Marketplace Opportunities. *Inf. Disp.* **37**, 18–23 (2021).
12. Konstantatos, G. *et al.* Ultrasensitive solution-cast quantum dot photodetectors. *Nature* **442**, 180–183 (2006).
13. McDonald, S. A. *et al.* Solution-processed PbS quantum dot infrared photodetectors and photovoltaics. *Nat. Mater.* **4**, 138–142 (2005).
14. Keuleyan, S., Lhuillier, E., Brajuskovic, V. & Guyot-Sionnest, P. Mid-infrared HgTe colloidal quantum dot photodetectors. *Nat. Photonics* **5**, 489–493 (2011).
15. Ackerman, M. M., Tang, X. & Guyot-Sionnest, P. Fast and Sensitive Colloidal Quantum Dot Mid-Wave Infrared Photodetectors. *ACS Nano* **12**, 7264–7271 (2018).
16. Zhang, H. *et al.* Material Perspective on HgTe Nanocrystal-Based Short-Wave Infrared Focal Plane Arrays. *Chem. Mater.* [acs.chemmater.2c02955](https://doi.org/10.1021/acs.chemmater.2c02955) (2022)
doi:10.1021/acs.chemmater.2c02955.
17. Liu, J. *et al.* A near-infrared colloidal quantum dot imager with monolithically integrated readout circuitry. *Nat. Electron.* 1–9 (2022) doi:10.1038/s41928-022-00779-x.
18. Goossens, S. *et al.* Broadband image sensor array based on graphene–CMOS integration. *Nat. Photonics* **11**, 366–371 (2017).
19. Livache, C. *et al.* A colloidal quantum dot infrared photodetector and its use for intraband detection. *Nat. Commun.* **10**, 2125 (2019).

20. Yang, H. *et al.* Au-Doped Ag₂Te Quantum Dots with Bright NIR-IIb Fluorescence for In Situ Monitoring of Angiogenesis and Arteriogenesis in a Hindlimb Ischemic Model. *Adv. Mater.* **n/a**, 2103953.
21. Zhang, Y. *et al.* Controlled Synthesis of Ag₂Te@Ag₂S Core–Shell Quantum Dots with Enhanced and Tunable Fluorescence in the Second Near-Infrared Window. *Small* **16**, 2001003 (2020).
22. Chen, C., He, X., Gao, L. & Ma, N. Cation Exchange-Based Facile Aqueous Synthesis of Small, Stable, and Nontoxic Near-Infrared Ag₂Te/ZnS Core/Shell Quantum Dots Emitting in the Second Biological Window. *ACS Appl. Mater. Interfaces* **5**, 1149–1155 (2013).
23. Liu, Z.-Y. *et al.* Breaking through the Size Control Dilemma of Silver Chalcogenide Quantum Dots via Trialkylphosphine-Induced Ripening: Leading to Ag₂Te Emitting from 950 to 2100 nm. *J. Am. Chem. Soc.* jacs.1c06661 (2021) doi:10.1021/jacs.1c06661.
24. Zhang, M.-Y. *et al.* Regulation of Silver Precursor Reactivity via Tertiary Phosphine to Synthesize Near-Infrared Ag₂Te with Photoluminescence Quantum Yield of up to 14.7%. *Chem. Mater.* acs.chemmater.1c02610 (2021) doi:10.1021/acs.chemmater.1c02610.
25. Chen, H. *et al.* Regulating surface potential maximizes voltage in all-perovskite tandems. *Nature* (2022) doi:10.1038/s41586-022-05541-z.
26. Shi, X.-H., Dai, Y.-Y., Wang, L., Wang, Z.-G. & Liu, S.-L. Water-Soluble High-Quality Ag₂Te Quantum Dots Prepared by Mutual Adaptation of Synthesis and Surface Modification for In Vivo Imaging. *ACS Appl. Bio Mater.* **4**, 7692–7700 (2021).
27. Yarema, M. *et al.* Infrared Emitting and Photoconducting Colloidal Silver Chalcogenide Nanocrystal Quantum Dots from a Silylamide-Promoted Synthesis. *ACS Nano* **5**, 3758–3765 (2011).
28. Wu, W., Schulman, J. N., Hsu, T. Y. & Efron, U. Effect of size nonuniformity on the absorption spectrum of a semiconductor quantum dot system. *Appl. Phys. Lett.* **51**, 710–712 (1987).
29. Liu, M. *et al.* Hybrid organic–inorganic inks flatten the energy landscape in colloidal quantum dot solids. *Nat. Mater.* **16**, 258–263 (2017).

30. Gilmore, R. H., Lee, E. M. Y., Weidman, M. C., Willard, A. P. & Tisdale, W. A. Charge Carrier Hopping Dynamics in Homogeneously Broadened PbS Quantum Dot Solids. *Nano Lett.* **17**, 893–901 (2017).
31. Kagan, C. R. & Murray, C. B. Charge transport in strongly coupled quantum dot solids. *Nat. Nanotechnol.* **10**, 1013–1026 (2015).
32. Aubert, T. *et al.* General Expression for the Size-Dependent Optical Properties of Quantum Dots. *Nano Lett.* **22**, 1778–1785 (2022).
33. Rodenkirchen, C. *et al.* Employing Interfaces with Metavalently Bonded Materials for Phonon Scattering and Control of the Thermal Conductivity in TAGS-x Thermoelectric Materials. *Adv. Funct. Mater.* **30**, 1910039 (2020).
34. Lee, M., Rosenbaum, T. F., Saboungi, M.-L. & Schnyders, H. S. Band-Gap Tuning and Linear Magnetoresistance in the Silver Chalcogenides. *Phys. Rev. Lett.* **88**, 066602 (2002).
35. Pei, Y., Heinz, N. A. & Snyder, G. J. Alloying to increase the band gap for improving thermoelectric properties of Ag₂Te. *J. Mater. Chem.* **21**, 18256 (2011).
36. Das, V. D. & Karunakaran, D. Semiconducting behavior of Ag₂Te thin films and the dependence of band gap on thickness. *J. Appl. Phys.* **54**, 5252–5255 (1983).
37. Yang, J. *et al.* Ligand-Engineered HgTe Colloidal Quantum Dot Solids for Infrared Photodetectors. *Nano Lett.* [acs.nanolett.2c00950](https://doi.org/10.1021/acs.nanolett.2c00950) (2022) doi:10.1021/acs.nanolett.2c00950.
38. Sun, B. *et al.* Fast Near-Infrared Photodetection Using III–V Colloidal Quantum Dots. *Adv. Mater.* **34**, 2203039 (2022).
39. Leemans, J. *et al.* Colloidal III–V Quantum Dot Photodiodes for Short-Wave Infrared Photodetection. *Adv. Sci.* **9**, 2200844 (2022).
40. Vafaie, M. *et al.* Colloidal quantum dot photodetectors with 10-ns response time and 80% quantum efficiency at 1,550 nm. *Matter* **4**, 1042–1053 (2021).
41. Biondi, M. *et al.* Facet-Oriented Coupling Enables Fast and Sensitive Colloidal Quantum Dot Photodetectors. *Adv. Mater.* **n/a**, 2101056 (2021).
42. Chen, D. *et al.* Passivating 100 Facets of PbS Colloidal Quantum Dots via Perovskite Bridges for Sensitive and Stable Infrared Photodiodes. *Adv. Funct. Mater.* **n/a**, 2210158.

43. Zhang, Y. *et al.* Electron Transport Layers Employing Strongly-Bound Ligands Enhance Stability in Colloidal Quantum Dot Infrared Photodetectors. *Adv. Mater.* **n/a**, 2206884 (2022).
44. Lu, S. *et al.* High-Performance Colloidal Quantum Dot Photodiodes via Suppressing Interface Defects. *ACS Appl. Mater. Interfaces* **15**, 12061–12069 (2023).

FIGURES

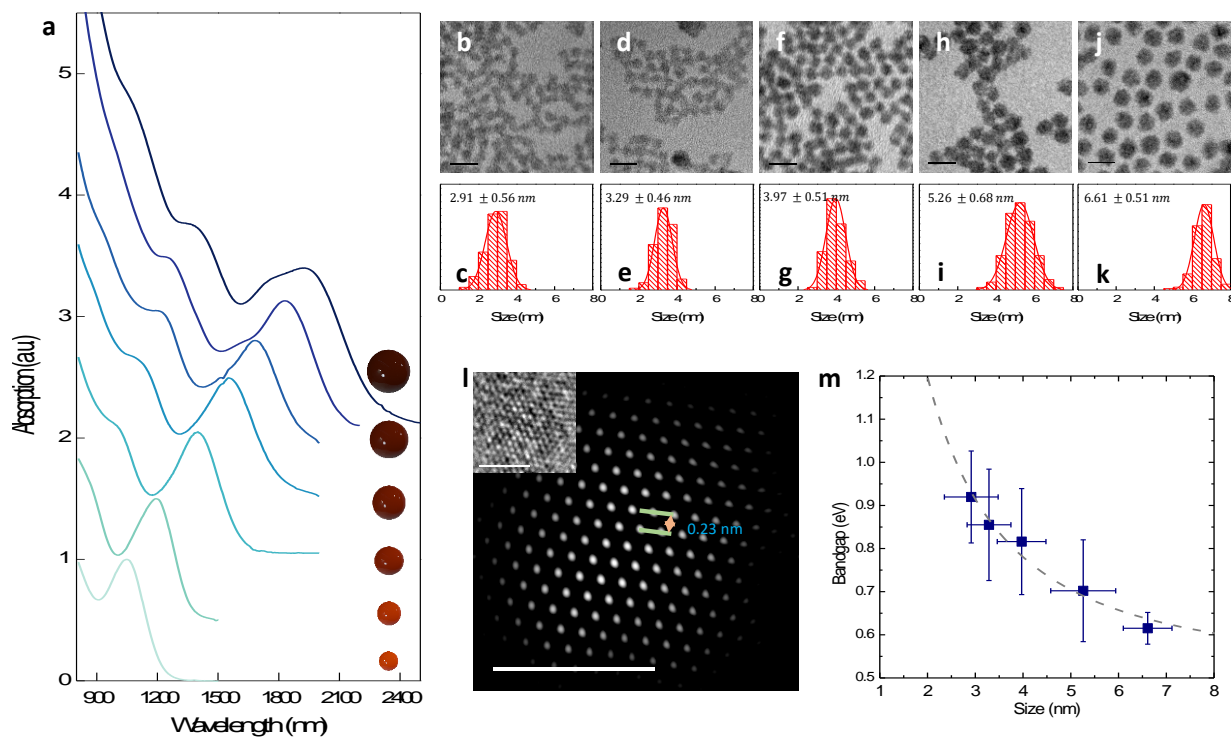


Fig. 1 | Size-tunable Ag₂Te QDs. **a**, Absorption spectrum of various sizes Ag₂Te QDs. Transmission electron microscope (TEM) images of Ag₂Te QDs with absorption peak at **b**, 1310 nm, **d**, 1430 nm, **f**, 1520 nm, **h**, 1750 nm, **j**, 1940 nm, and **c**, **e**, **g**, **i**, **k** their size distribution histograms, respectively. TEM sample grids, except the 1940 nm one, were immersed in methanol to remove organic residues for better resolution. **l**, High resolution TEM image of a single QD, showing single crystalline features. **m**, Sizing curve of Ag₂Te QDs from absorption peak positions and TEM size distribution. Dash line indicates the fitting line of first exciton peaks.

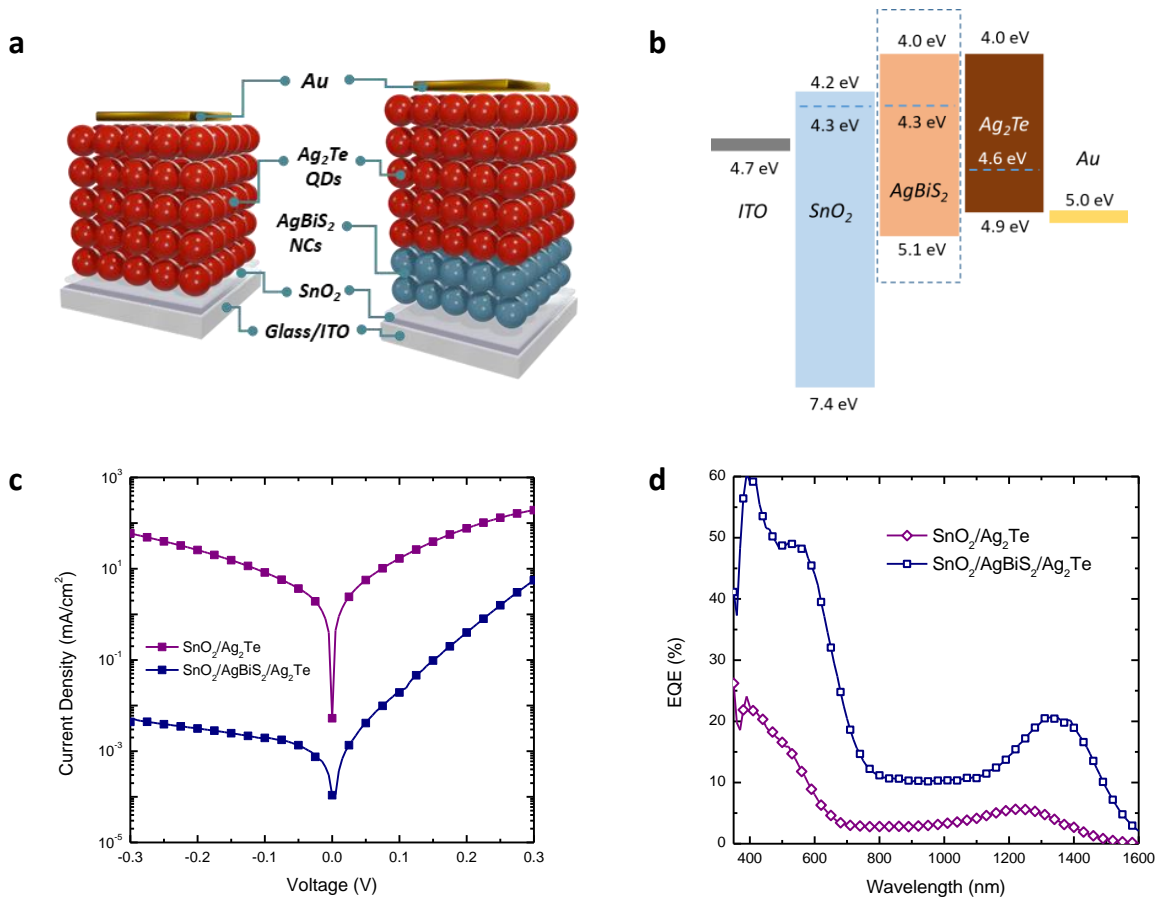


Fig. 2 | Ag₂Te QD Shortwave infrared photodiode. **a**, Schematics of Ag₂Te QD photodiodes, with and without AgBiS₂ NCs buffer layer. **b**, Band diagram of photodiode device. **c**, Dark current density-voltage (*J-V*) curves of photodiodes with and without buffer layer. **d**, External quantum efficiency (EQE) spectrum of Ag₂Te QD photodiode with and without AgBiS₂ NCs buffer layer.

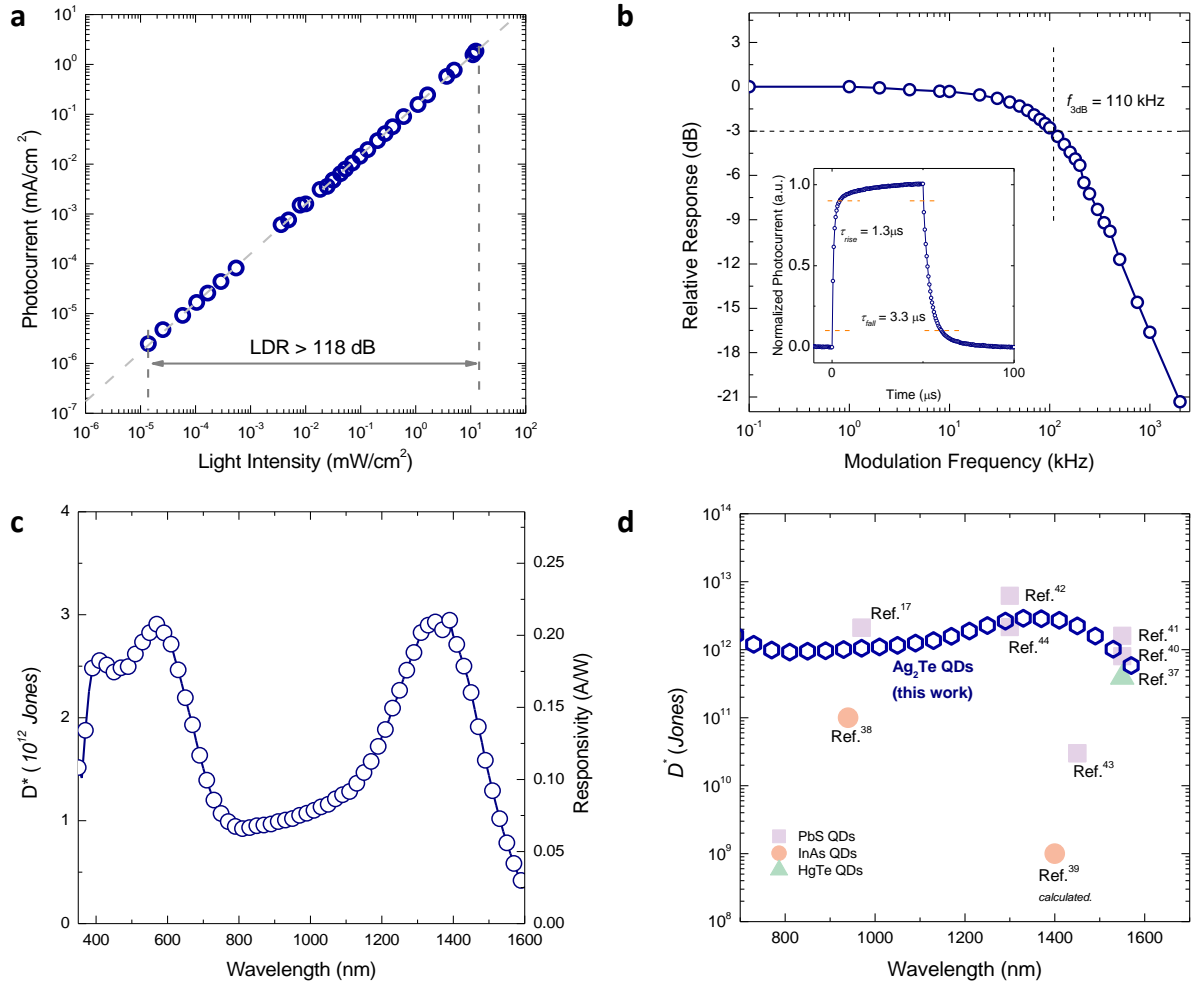


Fig. 3 | Performance of Ag₂Te QD photodiode. **a**, Linear dynamic range (LDR) of Ag₂Te QD photodiode under 1310nm pulse light illumination with power densities from ~ 10 nW/cm² to ~ 10 mW/cm². **b**, Response bandwidth of Ag₂Te QD photodiode. **c**, Specific detectivity spectrum at 20 kHz. **d**, Wavelength dependent specific detectivity of shortwave infrared photodiodes reported in literature.^{17,37–44}

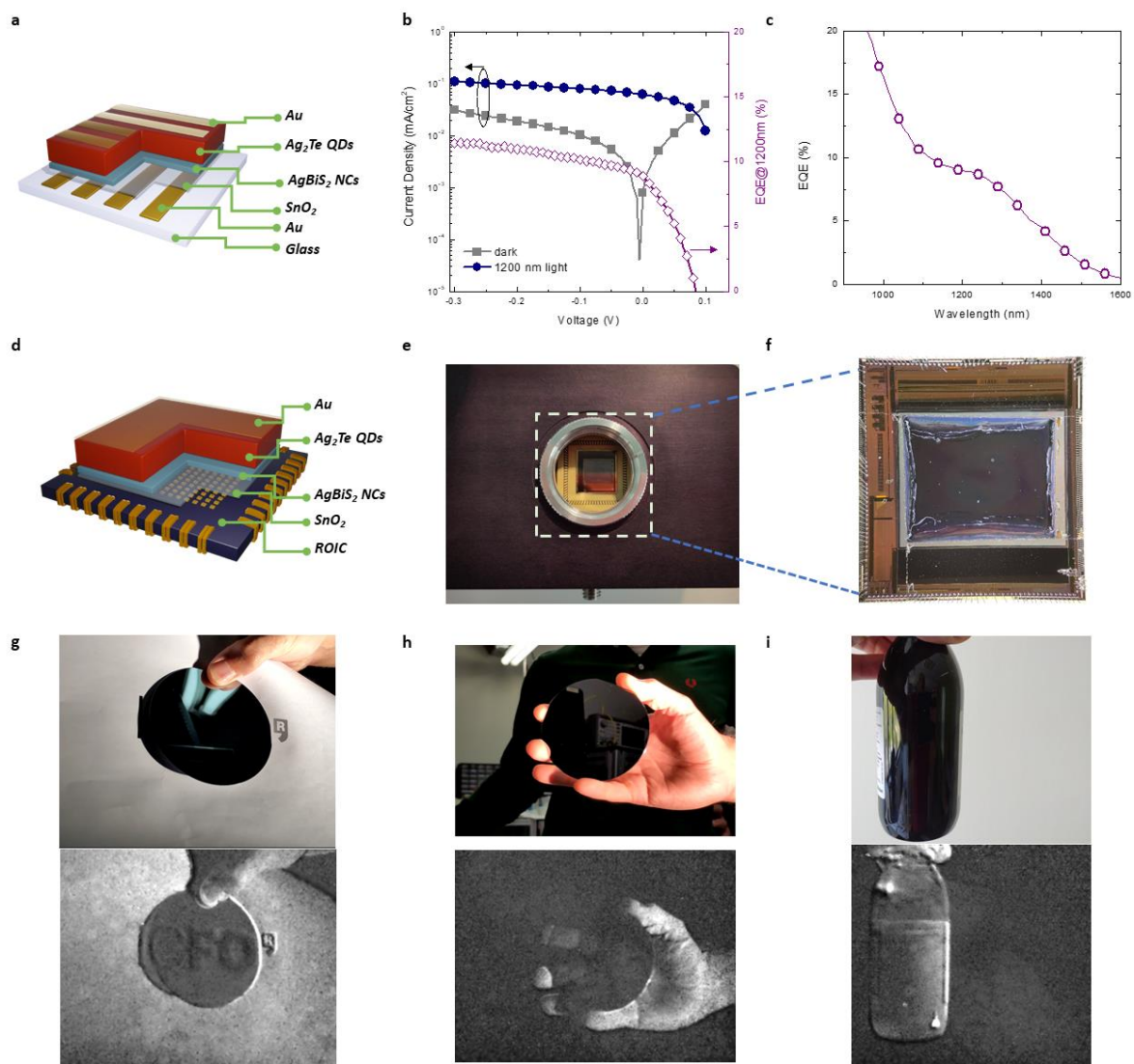


Fig. 4 | Top-illuminated Ag_2Te QD photodetector and imager. **a**, Schematic of top-illuminated Ag_2Te QD photodetector. **b**, Current density-voltage curves under dark and 0.7 mW/cm^2 1200 nm light illumination. **c**, EQE spectrum of top-illuminated device. **d**, Schematic of ROIC integrated Ag_2Te QDs SWIR imager. **e**, Photo of the imager and **f** zoom in of the ROIC die. **g**, Photos of a silicon wafer on ICFO logo with smartphone visible camera and Ag_2Te QD SWIR camera. **h**, photos of hand holding silicon wafer with visible camera and Ag_2Te QD SWIR camera. **i**, Photos of a dark bottle with liquid using smartphone visible camera and Ag_2Te QD SWIR camera.